fractal and fractional

MDPI

Article

Predicting the Remaining Useful Life of Turbofan Engines Using Fractional Lévy Stable Motion with Long-Range Dependence

Deyu Qi [1], Zijiang Zhu [1], Fengmin Yao [1], Wanqing Song [2,*], Aleksey Kudreyko [3], Piercarlo Cattani [4] and Francesco Villecco [5]

[1] Institute of Digitization Science and Technology, South China Business College, Guangdong University of Foreign Studies, No. 181, Liangtian Middle Road, Baiyun District, Guangzhou 510545, China; qideyu@gmail.com (D.Q.); 201017@gwng.edu.cn (Z.Z.); yaofm@vip.sina.com (F.Y.)
[2] School of Electronic and Electrical Engineering, Minnan University of Science and Technology, Quanzhou 362700, China
[3] Department of Medical Physics and Informatics, Bashkir State Medical University, Lenina 3, 450008 Ufa, Russia; akudreyko@bashgmu.ru
[4] Department of Computer, Control and Management Engineering, University of Rome La Sapienza, Via Ariosto 25, 00185 Roma, Italy; cattani.1642354@studenti.uniroma1.it
[5] Department of Industrial Engineering, University of Salerno, Via Giovanni Paolo II 132, 84084 Fisciano, Italy; fvillecco@unisa.it
* Correspondence: swqls@126.com

Abstract: Remaining useful life prediction guarantees a reliable and safe operation of turbofan engines. Long-range dependence (LRD) and heavy-tailed characteristics of degradation modeling make this method advantageous for the prediction of RUL. In this study, we propose fractional Lévy stable motion for degradation modeling. First, we define fractional Lévy stable motion simulation algorithms. Then, we demonstrate the LRD and heavy-tailed property of fLsm to provide support for the model. The proposed method is validated with the C-MAPSS dataset obtained from the turbofan engine. Principle components analysis (PCA) is conducted to extract sources of variance. Experimental data show that the predictive model based on fLsm with exponential drift exhibits superior accuracy relative to the existing methods.

Keywords: remaining useful life; self-similar; long-range dependence; fractional Lévy stable motion; feature fusion

Citation: Qi, D.; Zhu, Z.; Yao, F.; Song, W.; Kudreyko, A.; Cattani, P.; Villecco, F. Predicting the Remaining Useful Life of Turbofan Engines Using Fractional Lévy Stable Motion with Long-Range Dependence. *Fractal Fract.* **2024**, *8*, 55. https://doi.org/10.3390/fractalfract8010055

Academic Editors: Haci Mehmet Baskonus, Soheil Salahshour, Evren Hınçal, Kamyar Hosseini and Khadijeh Sadri

Received: 7 November 2023
Revised: 4 January 2024
Accepted: 11 January 2024
Published: 15 January 2024

1. Introduction

Developing algorithms and software modules that allow processing online data from IoT devices to predict turbofan engines' remaining useful life (RUL), i.e., the number of work cycles after the last completed cycle, is a relevant research topic. Remaining useful life prediction can effectively eliminate potential safety hazards of passenger flights [1]. The traditional approach to equipment maintenance involves a combination of breakdown and preventive maintenance [2]. The former means repairing and replacing equipment when it breaks down. The latter indicates the repairing of equipment prior to the failure, and the best timing of maintenance is chosen by the RUL prediction [3].

The degradation process of turbofan engines is related to environmental temperature, material, load changes, and other factors, making it difficult to predict the remaining useful life (RUL). Currently, the mainstream RUL prediction methods are artificial intelligence, stochastic model, and data-driven, based on acoustic monitoring of turbofan engines. The primary artificial intelligence algorithms utilized are LSTM and deep learning approaches. In recent years, various improved LSTM [4,5] and deep learning optimization algorithms [6–8] have been proposed to improve the accuracy of RUL prediction. These advancements also aim to combine both approaches [9,10], which necessitates a large number of data samples. The stochastic model method establishes a stochastic model

for the non-stationarity and randomness of the degradation process [11–13]. Data-driven research often needs as many data samples as possible combined with LSTM and deep learning [14,15].

Each of these methods has its advantages and disadvantages, but the biggest problem is that the prediction length of non-stationary time series is too short. The reason for the shortcoming is that the fundamentals of these algorithms are similar to the least squares fitting methods predictive models of RUL based on artificial intelligence, which aim to establish a mapping relationship between the monitoring dataset and the failure time. However, this relationship between the monitoring data and RUL is difficult to express clearly and is always implemented as a "black box" characteristic [16].

Additionally, a method exists that involves combining turbofan engine vibration signals and acoustic signals using a multi-sensor fusion to create a two-dimensional signal image [17–19]. Then, we can apply deep learning to predict the RUL. Deep learning is very mature in two-dimensional feature extraction. In practical applications, the fluctuations of aircraft engines during operation are too large, and thus, we hope that the incipient faults can be identified as early as possible. However, the current deep learning models are not sensitive and accurate enough.

Degradation is a slow and non-stationary stochastic process. The degradation sequence waveform exhibits characteristics of self-similarity and long-range dependence. This means each segment of the waveform is self-similar to the overall trend of change, and the degradation state at any given moment is closely related to its previous states; this property is known as long-range dependence. Based on this concept, the objective is to establish a non-stationary stochastic prediction model that possesses both self-similar and long-range dependent characteristics. The data series generated by this model will closely mimic the actual degradation sequences observed in the turbofan engine, resulting in high prediction accuracy and extended forecasting capability.

This paper proposes a non-stationary stochastic fractional-order Levy stable operation model, demonstrating its self-similarity and long-range dependence. By analyzing the collected time series data of turbofan engine vibrations, we utilize the Hurst exponent to determine the presence of long-range dependence. Subsequently, the model parameters are identified, ensuring that the series generated by the model highly resembles the degradation process of the turbofan engine. The model is trained with the principle components analysis (PCA) output.

A review of the Brownian motion (BM)-based RUL predictive examines several problems of this approach [20]. However, there are still some problems with the BM model. The BM model is a Markov process, but in practice, the aging data exhibit LRD [21]. The fractional Brownian motion extends the BM model to the fractional order. The fBm model introduces the LRD characteristics through the Hurst parameter. Song et al. developed a series of iterative differential predictive models based on the fBm model [22,23]. Gao et al. obtained the analytical expression of the probability density function (PDF) for the RUL prediction based on fBm [24]. In fact, Levy stable motion and fractional Brownian motion were applied to different studies [23,25–28].

This article is organized as follows: Section 2 proposes the fLsm model, and Section 3 provides LRD properties and self-similar characteristics of the fLsm model. The degradation model based on fLsm is presented in Section 4, and a case study with the C-MAPSS dataset is provided in Section 5 [29].

2. Fractional Lévy Stable Motion

2.1. Probability Density Function of the Lévy Stable Distribution

The connection between the generalized central limit theorem and Lévy stable distribution implies that the analytical expression of the PDF in the closed form does not

exist [30]. Therefore, the properties of the Lévy stable distribution are expressed by its characteristic function defined by $\varphi(\theta:\ \alpha,\ \beta,\ \delta,\ \mu)$, which is defined as follows:

$$\varphi(\theta:\alpha,\beta,\delta,\mu)=E\left[e^{j\theta x}\right]=\begin{cases} exp\left\{j\mu\theta-\delta|\theta|^{\alpha}\left[1-j\beta\frac{\theta}{|\theta|}tan\left(\frac{\pi\alpha}{2}\right)\right]\right\},\ \alpha\neq 1 \\ exp\left\{j\mu\theta-\delta|\theta|^{\alpha}\left[1+j\beta\frac{\theta}{|\theta|}\frac{2}{\pi}ln|\theta|\right]\right\},\ \alpha=1 \end{cases} \tag{1}$$

Usually, $X\sim S_{\alpha}(\beta,\mu,\delta)$ is used to indicate that the random variable follows the Lévy stable distribution, described by the characteristic exponent α, which measures the thickness of the tails of the distribution. β is the skew index, δ is the drift coefficient, and μ is the diffusion parameter. The shape of the distribution is governed by parameters α and β. Linear transformation of the distribution is determined by δ and μ. The parameters of Equation (1) must satisfy the following restrictions: $\alpha\in(0,2]$, $\beta\in[-1,1]$, $\mu\in\mathbb{R}$, $\delta>0$. The effect of the governing parameters on the PDF is shown in Figure 1.

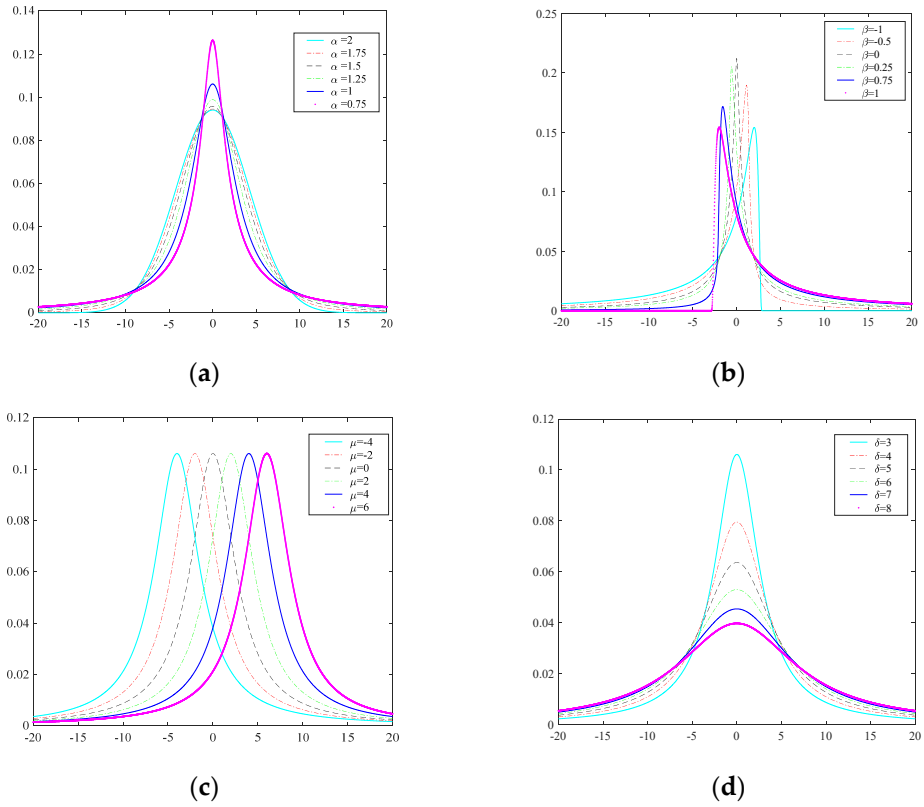

Figure 1. Probability density function. (**a**) Compare α in Levy stable; (**b**) different β in Levy stable; (**c**) influence of different coefficients μ; and (**d**) different parameter δ.

2.2. Fractional Lévy Stable Motion

fLsm is obtained by extending the Lévy stable motion into the fractional order based on the derivation of the fBm model. The fBm model can be simply described as:

$$B_H(t)\triangleq\frac{1}{\Gamma\left(H+\frac{1}{2}\right)}\left\{\int_{-\infty}^{0}\left[(t-u)^{H-\frac{1}{2}}-(-u)^{H-\frac{1}{2}}\right]\omega(u)du+\int_{0}^{t}(t-u)^{H-\frac{1}{2}}\omega(u)du\right\}, \tag{2}$$

where $0<H<1$ is the Hurst parameter, $\omega(u)$ is the Gaussian white noise with zero expectation, and $\Gamma(.)$ is the gamma function. Let us replace $H-\frac{1}{2}$ in Equation (2) with $H-\frac{1}{\alpha}$ and the Gaussian white noise with Lévy white noise. Then, the expression of the fLsm takes the form:

$$L_{H,\alpha}(t)=\int_{-\infty}^{+\infty}\left\{a\left[(t-s)_{+}^{H-\frac{1}{\alpha}}-(-s)_{+}^{H-\frac{1}{\alpha}}\right]+b\left[(t-s)_{-}^{H-\frac{1}{\alpha}}-(-s)_{-}^{H-\frac{1}{\alpha}}\right]\right\}Mds, \tag{3}$$

where $(x_+) = (-x)_- = \begin{cases} x, & x > 0 \\ 0, & x \leq 0 \end{cases}$, a and b are real constants, $|a|+|b|> 0$, and M is the Lévy stability measure in the Lebesgue measure space. Note that the fLsm model becomes the fBm model when $\alpha = 2$.

2.3. Simulation Algorithm

Fractional Lévy stable noise can be expressed as follows:

$$X_{H,\alpha} = D_t^{-a}\omega_a(t) = \frac{1}{\Gamma(a)}\int_0^t (t-s)^{a-1}\omega_a(s)ds, 0 < a < 0.5, \tag{4}$$

where $\omega_a(t)$ is the Lévy stable white noise and $X_{H,\alpha}$ denotes the generated fractional Lévy stable noise sequence. The fractional Lévy stable noise degenerates to fractional Gaussian noise when $\alpha = 2$.

The fractional Lévy stable noise is the incremental process of the fLsm model, so the simulation sequence of the fLsm model can be obtained by integrating or accumulating Equation (4) as follows:

$$L_{H,\alpha} = D_t^{-1}X_{H,\alpha} = \frac{1}{\Gamma(a+1)}\int_0^t (t-s)^{a}\omega_a(s)ds, 0 < a <0.5, \tag{5}$$

Figure 2 shows the simulated sequences of the fLsm for H = 0.8 and α = 1.4, 2.

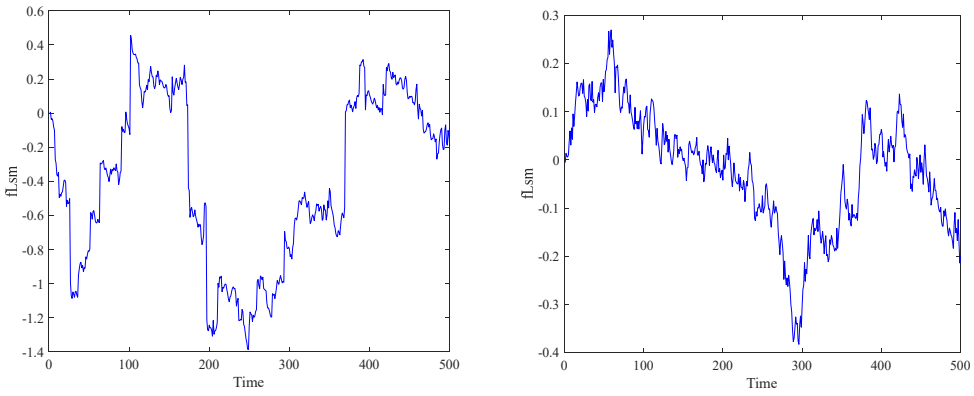

Figure 2. Simulation sequence of the fLsm model for H = 0.8 and α = 1.4, 2.0.

3. The Property of the fLsm

The self-similar nature of the fLsm is represented by parameter H ($H \neq 1/\alpha$) [31], and its LRD characteristic is given by the relationship between α and H:$\alpha H > 1$.

3.1. LRD Property

To ensure that the fLsm model effectively fits the LRD of stochastic sequences, we limit the range of parameters α and H to $\alpha \in (1, 2)$ and $H \in (1/2, 1)$, respectively.

$$L_{H,\alpha}(t) = \int_{-\infty}^{\infty} \left\{ a\left[(t-s)_+^{H-\frac{1}{\alpha}} - (-s)_+^{H-\frac{1}{\alpha}}\right] + b\left[(t-s)_-^{H-\frac{1}{\alpha}} - (-s)_-^{H-\frac{1}{\alpha}}\right] \right\} M_\alpha(ds), \tag{6}$$

Allowing us to derive the following equation can be derived:

① when $H = \frac{1}{\alpha}$, the value of fLsm is as follows:

$$L_{H,\alpha}(t) = \int_{-\infty}^{\infty} (a-b)M_\alpha(ds), \tag{7}$$

if a and b are constants, then the $L_{H,\alpha}(t)$ series is mutually independent without any relativity.

② when $H < \frac{1}{\alpha}$, the fLsm integration kernel includes all the states of the past time, but the integration is inversely proportional to the past states; therefore, the predicted results are inversely proportional to the actual results. This is called short-range dependence (SRD).

③ when $H > \frac{1}{\alpha}$, the fLsm integration kernel contains all the states of the past time s, but the integration is directly proportional to the past state; this is called long-range dependence (LRD).

The LRD properties of the fLsm model are determined by H and α. The larger the product, the stronger the LRD properties. Special note $0 < \alpha \leq 1$: the fLsm model does not have LRD characteristics because H is limited to the interval $(0, 1)$, as shown in Figure 3.

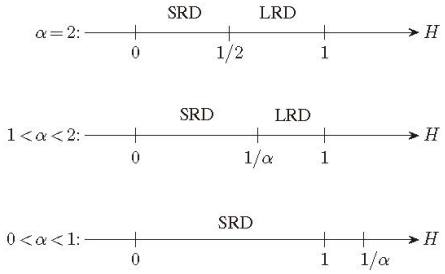

Figure 3. Dependence of the fLsm model.

3.2. Self-Similarity Property

A stochastic time series $X(t)$ is defined as having the following characteristics below:

$$X(t) \overset{d}{\Rightarrow} X(ct) \overset{d}{\Rightarrow} c^H X(t), \tag{8}$$

Furthermore, $X(t)$ is referred to as a self-similar process with exponent H.

The fLsm model is presented below:

$$L_{H,\alpha}(t) = \int_{-\infty}^{t} (a(t-s)^{H-\frac{1}{\alpha}} - bs^{H-\frac{1}{\alpha}}) M(ds), \tag{9}$$

For any $n \geq 1$, the series $M(\Delta_1), M(\Delta_2), \cdots, M(\Delta_n)$ are mutually independent and $\Delta_1, \Delta_2, \cdots, \Delta_n$ are mutually disjoint. Therefore, the series can be expressed using the self-similar parameter $H = \frac{1}{2}$:

$$M(cds) = c^{\frac{1}{2}} M(ds), \tag{10}$$

From (9) and (10), we obtain:

$$\begin{aligned} L_{H,\alpha}(ct) &= \textstyle\int_{-\infty}^{ct} \left(a(ct-s)^{H-\frac{1}{\alpha}} - bs^{H-\frac{1}{\alpha}}\right) M(ds) \\ &= c^{H-\frac{1}{\alpha}+\frac{1}{2}} \textstyle\int_{-\infty}^{t} (a(t-s)^{H-\frac{1}{\alpha}} - bs^{H-\frac{1}{\alpha}}) M(ds) = c^{H-\frac{1}{\alpha}+\frac{1}{2}} L_{H,\alpha}(t), \end{aligned} \tag{11}$$

Fundamentally, fLsm is a self-similar process characterized by the parameter $H - \frac{1}{\alpha} + \frac{1}{2}$.

4. Degradation Modeling of Fractional Lévy Stable Motion

4.1. Model Derivation

Lévy movement is the Brownian movement extend. In terms of the Langevin equation, the degradation model based on the fBm model is defined as follows:

$$dX(t) = \mu_B dt + \delta_B dB_H(t), \tag{12}$$

where $\{X(t), t \geq 0\}$ is the degradation process and μ_B is the coefficient of the drift term, which describes the degradation speed rate; the term occupies a dominant position. δ_B is the coefficient of the diffusion term, which describes the stochastic and LRD characteristics. $\{B_H(t), t \geq 0\}$ is the standard fBm model. $dB_H(t)$ is an increment.

$dL_{H,\alpha}(t)$ replaces $dB_H(t)$ so that we obtain

$$dX(t) = \mu_B dt + \delta_B dL_{H,\alpha}(t), \tag{13}$$

μ_B is a time-varying function $\mu(t;\theta)$, which is called drift function; θ is the parameter vector in the drift function, and $\int_0^t \mu(t;\theta)dt$ can change as demonstrated below:

$$\int_0^t \mu(t;\theta)dt = \mu\phi(t), \tag{14}$$

$\phi(t)$ usually has three defined functions: linear, nonlinear, and exponential power rate. The iterative degradation model based on the fLsm is represented as follows:

$$X(t_k + \Delta t_k) = X(t_k) + \int_{t_k}^{t_k+\Delta t_k} \mu(s;\theta)ds + \delta\omega(\Delta t_k), \tag{15}$$

$$\omega(\Delta t_k) = L_{H,\alpha}(t_k + \Delta t_k) - L_{H,\alpha}(t_k), \tag{16}$$

As a self-similar stochastic process, the following condition is satisfied for fLsm:

$$L_{H,\alpha}(at) - L_{H,\alpha}(0) \triangleq a^H[L_{H,\alpha}(t) - L_{H,\alpha}(0)], \tag{17}$$

and according to the Maruyama model:

$$\int_0^t f(\tau)(d\tau)^a = a\int_0^\tau (t-\tau)^{a-1} f(\tau)d\tau, \tag{18}$$

$$dx = f(t)(dt)^a, \tag{19}$$

Then, it can be concluded that:

$$L_{H,\alpha}(t_k + \Delta t_k) - L_{H,\alpha}(t_k) = \omega_\alpha(t)(\Delta t_k)^{H-\frac{1}{2}+\frac{1}{\alpha}}, \tag{20}$$

where $\omega_\alpha(t)$ is the Lévy white noise conforming to $S_\alpha(0,1,0)$.

Therefore, the iterative form of the degradation model is transformed into:

$$X(t_k + \Delta t_k) - X(t_k) = \int_{t_k}^{t_k+\Delta t_k} \mu(s;\theta)ds + \delta\omega_\alpha(t)(\Delta t_k)^{H-\frac{1}{2}+\frac{1}{\alpha}}, \tag{21}$$

Assume that $\alpha = 1.75$, $\beta = 0$, $\delta = 0.195$, $H = 0.75$, $\Delta t_k = 2$, and the simulation time is 100. Figure 4 presents the simulated degradation path.

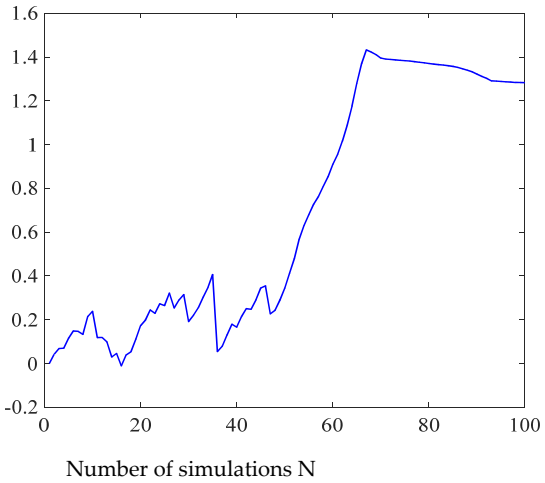

Figure 4. Numerical simulation of the degradation model.

4.2. Parameters Estimation

The Hurst parameter H plays a key role in the modeling process of fLsm. The rescaled range method is the most widely used Hurst parameter estimation algorithm. Therefore, we propose to adopt the rescaled range method to calculate the Hurst parameter.

Other parameters of fLsm are estimated by the improved eigenfunction-based method. The steps are shown in Figure 5.

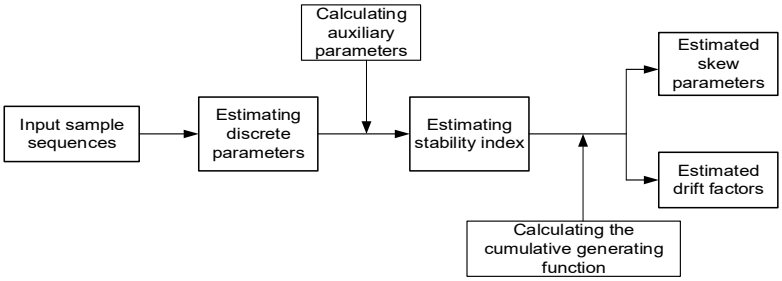

Figure 5. Flow chart of new characteristic function method.

The proposed eigenfunction method first calculates diffusion parameter δ. This procedure allows the value of the diffusion parameter δ to be estimated directly without the need to base it on the other three parameters. In addition, there are two auxiliary points to note in the estimation process of the new eigenfunction method: $\theta = 1$ and θ_0. One is the auxiliary point located at $\theta = 1$. This is because the absolute value of the eigenfunction at $\theta = 1$ is equal regardless of the value taken for the parameters of the eigenfunction:

$$|\varphi(\theta;\alpha,\beta,\mu,\delta)| = e^{-\delta|\theta|^{\alpha}}|_{\theta=1} = e^{-\delta}, \tag{22}$$

The second is the auxiliary parameter θ_0, which is introduced to calculate the estimate of the stability index α and can be obtained with the help of the diffusion parameter δ.

In order to estimate the diffusion parameter δ of the sample sequence $\{X(t), t = 1, 2, 3, \cdots\}$, the eigenfunction of Equation (23) can be considered as a complex function associated with θ.

$$|\varphi(\theta;\alpha,\beta,\mu,\delta)| = \left|E\left\{e^{j\theta x}\right\}\right| = e^{-\delta|\theta|^{\alpha}}, \tag{23}$$

Then, the logarithm is found for each side of Equation (23).

$$ln|\varphi(\theta;\alpha,\beta,\mu,\delta)| = -\delta|\theta|^{\alpha}, \tag{24}$$

Calculate the value of Equation (24) assuming $\theta = 1$ to obtain an estimate of the diffusion parameter δ.

$$\delta = -ln|\varphi(1;\alpha,\beta,\mu,\delta)| = -ln\left|E\left\{e^{jx}\right\}\right|, \tag{25}$$

The estimated value of the diffusion parameter δ is given by the following equation.

$$\hat{\delta} = -ln|\hat{\varphi}(1;\alpha,\beta,\mu,\delta)| = -ln\frac{1}{N}\left|\sum_{i=1}^{N} e^{jx_i}\right|, \tag{26}$$

Before calculating the estimate of the stability index α and the second auxiliary parameter θ_0 needs to be calculated in addition to the known auxiliary point $\theta = 1$. The characteristic functions can degenerate to different models when the stability index α equals different values. Therefore, the new eigenfunction method uses the Cauchy and Gaussian eigenfunctions corresponding to $\alpha = 1$ and $\alpha = 2$ to calculate the auxiliary parameter θ_0.

This is carried out by calculating the maximum distance between the absolute values of the Cauchy eigenfunction $e^{-\delta\theta}$ and the Gaussian eigenfunction $e^{-\delta\theta^2}$.

$$\frac{d}{d\theta}\left|e^{-\delta\theta^2} - e^{-\delta\theta}\right| = 0, \tag{27}$$

$$2\theta e^{-\delta\theta^2} = e^{-\delta\theta}, \tag{28}$$

Taking the logarithm of Equation (28) yields the following Equation (29).

$$\frac{ln2\theta}{\theta^2 - \theta}|_{\theta_0} = \hat{\delta}, \tag{29}$$

The value of the auxiliary parameter θ_0 is obtained by solving Equation (29). Substituting the obtained θ_0 into Equations (24) and (25):

$$\theta_0^{\alpha} = \frac{ln\left|E\left\{e^{j\theta_0 x}\right\}\right|}{ln\left|E\left\{e^{jx}\right\}\right|} = \frac{ln|\hat{\varphi}(\theta_0;\alpha,\beta,\mu,\delta)|}{ln|\hat{\varphi}(1;\alpha,\beta,\mu,\delta)|}, \tag{30}$$

Therefore, the estimated value of the stability index α can be expressed as:

$$\hat{\alpha} = \frac{\frac{ln|\hat{\varphi}(\theta_0;\alpha,\beta,\mu,\delta)|}{ln|\hat{\varphi}(1;\alpha,\beta,\mu,\delta)|}}{ln\theta_0} * log_{\theta_0}\left(\frac{ln|\hat{\varphi}(\theta_0;\alpha,\beta,\mu,\delta)|}{ln|\hat{\varphi}(1;\alpha,\beta,\mu,\delta)|}\right), \tag{31}$$

where $\hat{\varphi}(\theta_0;\alpha,\beta,\mu,\delta) = \frac{1}{N}\left|\sum_{i=1}^{N} e^{j\theta_0 x_i}\right|$.

The estimates of skewness index β and drift coefficient μ are calculated from the logarithmic form of the characteristic function.

$$ln|\varphi(\theta;\alpha,\beta,\mu,\delta)| = -\delta|\theta|^{\alpha} + j\left[\delta|\theta|^{\alpha}\beta\frac{\theta}{|\theta|}tan\left(\frac{\pi\alpha}{2}\right) + \mu\theta\right], \tag{32}$$

Suppose $\theta = 1$, then Equation (32) can be expressed as:

$$\ln\varphi(1;\alpha,\beta,\mu,\delta) = -\delta + j\left[\delta\beta tan\left(\frac{\pi\alpha}{2}\right) + \mu\right], \tag{33}$$

Equation (33) reveals that the estimated value of the diffusion parameter can be expressed in terms of the real part. This is expressed as follows:

$$\hat{\delta} = -Re\{\ln\hat{\varphi}(1;\alpha,\beta,\mu,\delta)\}, \tag{34}$$

Furthermore, considering $\ln y = \ln|y| + jarg(y + 2k\pi)$, we can obtain:

$$Re\{\ln\hat{\varphi}(1;\alpha,\beta,\mu,\delta)\} = \ln|\hat{\varphi}\ (1;\alpha,\beta,\mu,\delta)|, \tag{35}$$

$$Im\{\ln\hat{\varphi}(1;\alpha,\beta,\mu,\delta)\} = \arg\hat{\varphi}(1;\alpha,\beta,\mu,\delta), \tag{36}$$

Considering the two auxiliary parameters $\theta = 1$ and θ_0, one can solve Equations (35) and (36) to obtain the skewness index β and the drift coefficient μ.

$$\hat{\beta} = \frac{Im\{\ln|\hat{\varphi}\ (\theta_0;\alpha,\beta,\mu,\delta)| - \theta_0\ln|\hat{\varphi}\ (1;\alpha,\beta,\mu,\delta)|\}}{\hat{\delta}tan\left(\frac{\pi\hat{\alpha}}{2}\right)({\theta_0}^{\alpha} - \theta_0)}, \tag{37}$$

$$\hat{\mu} = \frac{Im\left\{{\theta_0}^{\hat{\alpha}}\ln|\hat{\varphi}\ (1;\alpha,\beta,\mu,\delta)| - \ln|\hat{\varphi}\ (\theta_0;\alpha,\beta,\mu,\delta)|\right\}}{{\theta_0}^{\alpha} - \theta_0}, \tag{38}$$

5. Case Study

The datasets consist of multiple multi-dimensional time series data. Each data set is divided into training and test samples. A separate time series comes from different engines of the same type and represents changes in various characteristics: pressure, temperature, equipment rotation speeds, etc. Systems start up with different degrees of initial wear and production changes. Each engine has 21 sensors that collect various measurements related to the engine's condition during operation. The engine runs normally at the beginning of each time series, and a malfunction occurs at some point during the series. The error grows in magnitude in the training set until the system crashes. The proposed method was applied to the subset FD001 of the C-MAPSS dataset [29] for aero-engine unit prognostics. A schematic representation of the engine is depicted in Figure 6.

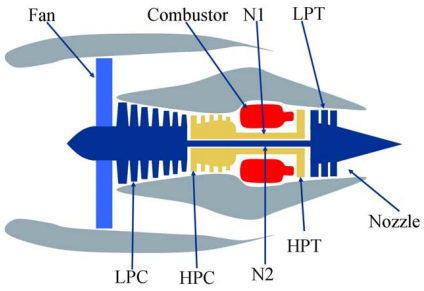

Figure 6. Schematic diagram of engine structure.

5.1. Feature Selection of Health Indicators

The subset FD001 varies in operating and fault conditions, and the data are contaminated with sensor noise. Therefore, we applied filtering to the training data. The filtering was carried out using the smooth filter function in MATLAB with a setting window of 10. Since there are considerable differences between the magnitudes of the data, we applied normalization to the data after filtering. In order to enhance degradation features, we applied PCA and fusion in the construction of HI (Figures 7 and 8).

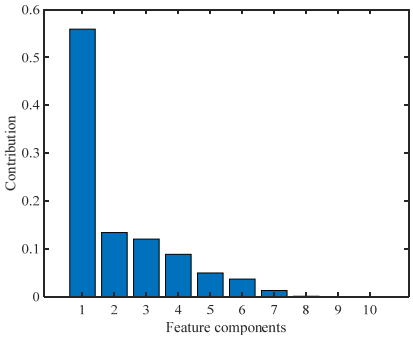

Figure 7. Results of principal component analysis.

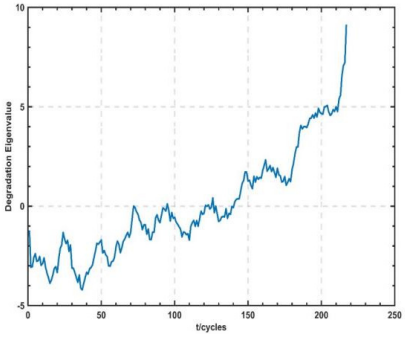

Figure 8. Engine health indicator after fusion.

5.2. Prediction of Remaining Useful Life

The definition of RUL is given as

$$T = inf\{t_k : X(t_k) \geq \omega | X(t_0) < \omega\}, \tag{39}$$

where ω indicates the degradation threshold. The non-Gaussian nature of fLsm makes it impossible to obtain the analytical formulas for the RUL prediction; therefore, we refer to the Monte Carlo method [32,33]. The point RUL prediction is the mode of a large number of RUL simulations [34,35]. The empirical threshold value ω was set to be 4.25. The fLsm model with three drift terms was chosen. The corresponding parameters are listed in Table 1. The corresponding results of RUL are shown in Figure 9.

Table 1. Input parameter of the fLsm model for different degradation trends.

Model	H	α	β	μ	δ
M_1	0.8669	1.7019	0.0686	1.3723	1.9623
M_2	0.8669	1.9473	0.0700	1.2531	2.0652
M_3	0.8669	1.9564	0.0715	1.3275	1.9514

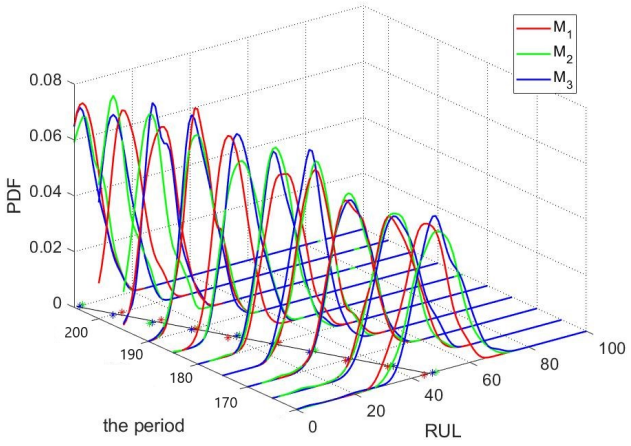

Figure 9. PDF estimation of the prediction model RUL with three different drift terms.

We use four standard error evaluation metrics to compare the predictive accuracy: mean absolute error, root mean square error, mean absolute percentage error, and Health Degree [36].

$$MAE = \frac{1}{m}\sum_{i=1}^{m}\left|r_i - r_i^*\right|, \tag{40}$$

$$RMSE = \sqrt{\frac{1}{m}\sum_{i=1}^{m}\left(r_i - r_i^*\right)^2}, \tag{41}$$

$$MAPE = \frac{1}{m}\sum_{i=1}^{m}\left|\frac{r_i - r_i^*}{r_i^*}\right| \times 100\%, \tag{42}$$

$$HD = 1 - \frac{\sum_{i=1}^{m}\left(r_i - r_i^*\right)^2}{\sum_{i=1}^{m}\left(r_i - \bar{r}\right)^2}, \tag{43}$$

where r_i denotes the predicted value of the RUL, which is obtained for the i-th prediction starting point. r_i^* is the actual value of the RUL at the i-th prediction starting point, m is the number of predictions, and $\bar{r}$ denotes the mean value of r_i. The results of error estimation are given in Table 2. As we can see, the exponential drift term of model M3 is superior to the power drift term of model M2 and the linear drift term M1.

Table 2. Prediction accuracy of RUL.

Model	MAE	RMSE	MAPE	HD
M_1	1.5000	1.6432	0.0147	0.9869
M_2	1.3000	1.4491	0.0153	0.9898
M_3	1.2000	1.3416	0.0054	0.9913

The fLsm model with an exponential drift is compared with the fGC model [37,38], the fBm model [22,23], and the LSTM model [39]. The results are shown in Figure 10. The LSTM neural network uses a single-input–single-output model with 200 hidden units in LSTM layers, a stacking layer of 2, and an initial learning rate of 0.005. The results of error estimation are shown in Table 3. Thus, the proposed approach outperformed other predictive models.

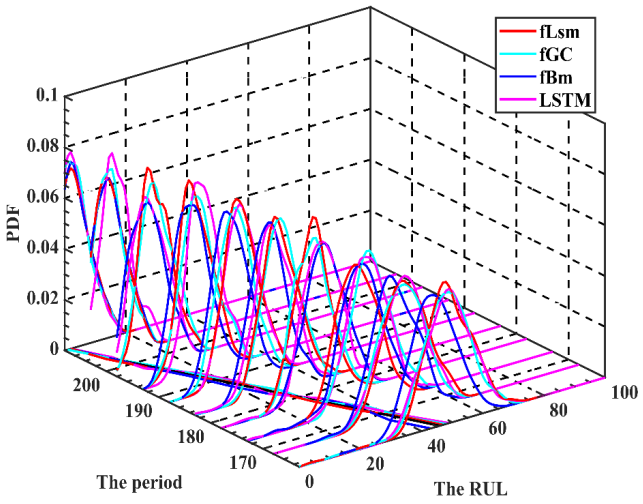

Figure 10. RUL prediction results for different degradation models.

Table 3. Prediction accuracy of RUL.

Model	MAE	RMSE	MAPE	HD
fLsm	1.2000	1.3416	0.0054	0.9913
fGC	1.4000	1.5632	0.0151	0.9893
fBm	1.6000	1.8439	0.0373	0.9815
LSTM	1.9000	1.9748	0.0476	0.9811

6. Conclusions

This paper proposes an iterative degradation model based on fLsm with LRD and heavy-tailed characteristics. We have also demonstrated that fLsm has LRD property and a heavy probabilistic tail. The RUL prediction is based on the Monte Carlo simulation of the degradation model, which is the Langevin-type stochastic differential equation driven by fLsm. A new eigenfunction method and rescaled range method were applied for the parameter identification of the model.

The model's training data, i.e., the HI, underwent PCA analysis, identifying degradation features and enabling us to construct HI using the dimension reduction PCA algorithm. The proposed model with an exponential drift is compared with the fGC, fBm, and the LSTM model. Real turbofan engine data were used for the case study, and the results indicate the advantage of the fLsm prediction model over other methods. We may utilize a more advanced drift term in the RUL prediction model based on fLsm.

In the future study, we will expand application fields, and the prediction accuracy and prediction length in time will be further improved by parameter optimization [40,41].

Author Contributions: Conceptualization, D.Q. and W.S.; methodology, W.S.; software, Z.Z. and F.Y.; validation, D.Q., Z.Z. and F.Y.; formal analysis, W.S.; data curation, P.C.; writing—original draft preparation, D.Q. and F.V.; writing—review and editing, A.K.; visualization, P.C. and F.V.; supervision, W.S.; project administration, D.Q. All authors have read and agreed to the published version of the manuscript.

Funding: The contribution of A. Kudreyko was supported by Bashkir State Medical University (Grand No. PRIORITY-2030).

Data Availability Statement: No new data were created or analyzed in this study. Data sharing is not applicable to this article.

Conflicts of Interest: The authors declare no conflicts of interest. The funders had no role in the design of this study, in the collection, analyses, or interpretation of data, in the writing of the manuscript, or in the decision to publish the results.

Abbreviations

fLsm	fractional Lévy stable Motion
fBm	Fractional Brownian Motion
fGC	Fractional Generalized Cauchy
HI	Health Indicator
LSTM	Long Short-Term Memory Neural Networks
LRD	Long-Range Dependence
SRD	Short-Range Dependence
MAE	Mean Absolute Error
MAPE	Mean Absolute Percentage Error
PDF	Probability Density Function
RMSE	Root Mean Square Error
RUL	Remaining Useful Life
HD	Health Degree
PCA	Principal Components Analysis

References

1. Lu, F.; Huang, J.; Xing, Y. Fault Diagnostics for Turbo-Shaft Engine Sensors Based on a Simplified On-Board Model. *Sensors* **2012**, *12*, 11061–11076. [CrossRef]
2. Lee, C.; Cao, Y.; Ng, K.H. Big data analytics for predictive maintenance strategies. In *Supply Chain Management in the Big Data Era*; IGI Global: Hershey, PA, USA, 2017; pp. 50–74. [CrossRef]
3. Chen, J.; Pan, J.; Li, Z.; Zi, Y.; Chen, X. Generator bearing fault diagnosis for wind turbine via empirical wavelet transform using measured vibration signals. *Renew. Energy* **2016**, *89*, 80–92. [CrossRef]
4. Hu, L.; He, X.; Yin, L. Remaining useful life prediction method combining the life variation laws of aero-turbofan engine and auto-expandable cascaded LSTM model. *Appl. Soft Comput.* **2023**, *147*, 110836. [CrossRef]
5. Tian, H.X.; Yang, L.Z.; Ju, B.T. Spatial correlation and temporal attention-based LSTM for remaining useful life prediction of turbofan engine. *Measurement* **2023**, *214*, 112816. [CrossRef]
6. Li, R.Z.; Zhan, H.F.; Han, K. A lightweight transformer and depthwise separable convolution model for remaining useful life prediction of turbofan engines. *Meas. Sci. Technol.* **2024**, *35*, 025020. [CrossRef]
7. Thakkar, U.; Chaoui, H. Remaining Useful Life Prediction of an Aircraft Turbofan Engine Using Deep Layer Recurrent Neural Networks. *Actuators* **2022**, *11*, 67. [CrossRef]
8. Wang, Y.M.; Wang, Y. Adenoising semi-supervised deep learning model for remaining useful life prediction of turbofan engine degradation. *Appl. Intell.* **2023**, *53*, 22682–22699. [CrossRef]
9. Li, J.; Jia, Y.; Niu, M.; Zhu, W.; Meng, F. Remaining Useful Life Prediction of Turbofan Engines Using CNN-LSTM-SAM Approach. *IEEE Sens. J.* **2023**, *23*, 10241–10251. [CrossRef]
10. Zheng, Y.; Bao, X.Y.; Wang, H.T. Prediction of Remaining Useful Life Using Fused Deep Learning Models: A Case Study of Turbofan Engines. *J. Comput. Inf. Sci. Eng.* **2022**, *22*, 054501. [CrossRef]
11. Mitici, M.; de Pater, I.; Zeng, Z.G. Dynamic predictive maintenance for multiple components using data-driven probabilistic RUL prognostics: The case of turbofan engines. *Reliab. Eng. Syst. Saf.* **2023**, *234*, 109199. [CrossRef]
12. Esfahani, Z.; Salahshoor, K.; Mazinan, A.H. Remaining useful life prognostics based on stochastic degradation modeling: Turbofan engine as case study. *J. Braz. Soc. Mech. Sci. Eng.* **2022**, *44*, 262. [CrossRef]
13. Wang, H.R.; Li, D.W.; Zhu, G.F. Remaining Useful Life Prediction of Aircraft Turbofan Engine Based on Random Forest Feature Selection and Multi-Layer Perceptron. *Appl. Sci.* **2023**, *13*, 7186. [CrossRef]

14. He, J.J.; Zhao, Y.P. An improved prognostics model with its application to the remaining useful life of turbofan engine. *Proc. Inst. Mech. Eng. Part G-J. Aerosp. Eng.* **2022**, *236*, 2108–2130. [CrossRef]
15. Xue, B.; Xu, Z.B.; Huang, X.; Nie, P.C. Data-driven prognostics method for turbofan engine degradation using hybrid deep neural network. *J. Mech. Sci. Technol.* **2021**, *35*, 5371–5387. [CrossRef]
16. Zhu, X.Y.; Chen, Z.Q.; Borgonovo, E. Remaining-useful-lifetime and system-remaining-profit based importance measures for decisions on preventive maintenance. *Reliab. Eng. Syst. Saf.* **2021**, *216*, 107951. [CrossRef]
17. Ren, L.; Wang, H.T.; Zhang, L. Time-Varying Gaussian Encoder-Based Adaptive Sensor-Weighted Method for Turbofan Engine Remaining Useful Life Prediction. *IEEE Trans. Instrum. Meas.* **2023**, *72*, 3522411. [CrossRef]
18. Sharanya, S.; Venkataraman, R.; Murali, G. Predicting remaining useful life of turbofan engines using degradation signal based echo state network. *Int. J. Turbo Jet Engines* **2022**, 3. [CrossRef]
19. Chen, X.; Zeng, M. Convolution-Graph Attention Network With Sensor Embeddings for Remaining Useful Life Prediction of Turbofan Engines. *IEEE Sens. J.* **2023**, *23*, 15786–15794. [CrossRef]
20. Zhang, Z.; Si, X.; Hu, C.; Lei, Y. Degradation data analysis and remaining useful life estimation: A review on Wiener-process-based methods. *Eur. J. Oper. Res.* **2018**, *271*, 775–796. [CrossRef]
21. Lei, Y.Y.; Li, N.; Jia, F.; Lin, J.; Xing, S. A nonlinear degradation model based method for remaining useful life prediction of rolling element bearings. In Proceedings of the 2015 Prognostics and System Health Management Conference (PHM), Beijing, China, 21–23 October 2015; pp. 1–8. [CrossRef]
22. Song, W.; Cattani, C.; Chi, C.H. Multifractional Brownian motion and quantum-behaved particle swarm optimization for short term power load forecasting: An integrated approach. *Energy* **2020**, *194*, 116847. [CrossRef]
23. Song, W.; Li, M.; Li, Y.; Cattani, C.; Chi, C.H. Fractional Brownian motion: Difference iterative forecasting models. *Chaos Solitons Fractals* **2019**, *123*, 347–355. [CrossRef]
24. Song, W.; Liu, H.; Zio, E. Long-range dependence and heavy tail characteristics for remaining useful life prediction in rolling bearing degradation. *Appl. Math. Model.* **2022**, *102*, 268–284. [CrossRef]
25. El Hassouni, M.; Tafraouti, A.; Toumi, H.; Lespessailles, E.; Jennane, R. Fractional Brownian Motion and Geodesic Rao Distance for Bone X-ray Image Characterization. *IEEE J. Biomed. Health Inform.* **2016**, *21*, 1347–1359. [CrossRef]
26. Karasaridis, A.; Hatzinakos, D. Network heavy traffic modeling using α-stable self-similar processes. *IEEE Trans. Commun.* **2001**, *49*, 1203–1214. [CrossRef]
27. Duan, S.; Song, W.Q.; Zio, E.; Cattani, C.; Li, M. Product technical life prediction based on multi-modes and fractional Lévy stable motion. *Mech. Syst. Signal Process.* **2021**, *161*, 107974. [CrossRef]
28. Zou, H.-L.; Yu, Z.; Anh, V.; Ma, Y.-L. From standard alpha-stable Lévy motions to horizontal visibility networks: Dependence of multifractal and Laplacian spectrum. *J. Stat. Mech. Theory Exp.* **2018**, *2018*, 053403. [CrossRef]
29. Saxena, A.; Goebel, K.; Simon, D.; Eklund, N. Damage propagation modeling for aircraft engine run-to-failure simulation. In Proceedings of the 2008 International Conference on Prognostics and Health Management, Denver, CO, USA, 6–9 October 2008; pp. 1–9.
30. Zhang, S.T.; Kang, R.; Liu, Y.H. Remaining useful life prediction for degradation with recovery phenomenon based on uncertain process. *Reliab. Eng. Syst. Saf.* **2021**, *208*, 107440. [CrossRef]
31. Samorodnitsky, G.; Taqqu, M.S. Stable non-gaussian random processes: Stochastic models with infinite variance. *J. Am. Stat. Assoc.* **1996**, *90*, 805–806. [CrossRef]
32. Hong, G.; Song, W.; Gao, Y.; Zio, E.; Kudreyko, A. An Iterative Model of the Generalized Cauchy Process for Predicting the Remaining Useful Life of Lithium-ion Batteries. *Measurement* **2022**, *187*, 110269. [CrossRef]
33. Lemieux, C. *Monte Carlo and Quasi-Monte Carlo Sampling*; Springer: New York, NY, USA, 2009. [CrossRef]
34. Cheng, Y.; Zhu, H.; Hu, K.; Wu, J.; Shao, X.; Wang, Y. Reliability prediction of machinery with multiple degradation characteristics using double-Wiener process and Monte Carlo algorithm. *Mech. Syst. Signal Process.* **2019**, *134*, 106333. [CrossRef]
35. Yang, F.; Habibullah, M.S.; Zhang, T.; Xu, Z.; Lim, P.; Nadarajan, S. Health index-based prognostics for remaining useful life predictions in electrical machines. *IEEE Trans. Ind. Electron.* **2016**, *63*, 2633–2644. [CrossRef]
36. Liu, H.; Song, W.; Zio, E. Metabolism and difference iterative forecasting model based on long-range dependent and grey for gearbox reliability. *ISA Trans.* **2022**, *122*, 486–500. [CrossRef]
37. Liu, H.; Song, W.; Zhang, Y.; Kudreyko, A. Generalized cauchy degradation model with long-range dependence and maximum lyapunov exponent for remaining useful life. *IEEE Trans. Instrum. Meas.* **2021**, *70*, 3512812. [CrossRef]
38. Fu, S.; Zhang, Y.; Lin, L. Deep residual lstm with domain-invariance for remaining useful life prediction across domains. *Reliab. Eng. Syst. Saf.* **2021**, *216*, 108012. [CrossRef]
39. Cheng, Y.; Wu, J.; Zhu, H.; Or, S.W.; Shao, X. Remaining useful life prognosis based on ensemble long short-term memory neural network. *IEEE Trans. Instrum. Meas.* **2021**, *70*, 3503912. [CrossRef]

40. Sathiyaraj, T.; Balasubramaniam, P. Controllability and optimal control for a class of time-delayed fractional stochastic integro-differential systems. *Appl. Math. Optim.* **2020**, *84*, 2527–2554. [CrossRef]
41. Dhayal, R.; Malik, M.; Abbas, S.; Debbouche, A. Optimal controls for second-order stochastic differential equations driven by mixed-fractional Brownian motion with impulses. *Math. Methods Appl. Sci.* **2020**, *43*, 4107–4124. [CrossRef]